

THE SPECTRAL EVOLUTION OF THE FIRST GALAXIES. III. SIMULATED JAMES WEBB SPACE TELESCOPE SPECTRA OF REIONIZATION-EPOCH GALAXIES WITH LYMAN CONTINUUM LEAKAGE

ERIK ZACKRISSON^{1*}, CHRISTIAN BINGGELI¹, KRISTIAN FINLATOR², NICKOLAY Y. GNEDIN^{3,4,5}, JAN-PIETER PAARDEKOOPER⁶, IKKOH SHIMIZU⁷, AKIO K. INOUE⁸, HANNES JENSEN¹, GENOVEVA MICHEVA⁹, SADEGH KHOCHFAR¹⁰ & CLAUDIO DALLA VECCHIA^{11,12}

ABSTRACT

Using four different suites of cosmological simulations, we generate synthetic spectra for galaxies with different Lyman continuum escape fractions (f_{esc}) at redshifts $z \approx 7-9$, in the rest-frame wavelength range relevant for the James Webb Space Telescope (JWST) NIRSpec instrument. By investigating the effects of realistic star formation histories and metallicity distributions on the EW(H β)- β diagram (previously proposed as a tool for identifying galaxies with very high f_{esc}), we find that neither of these effects are likely to jeopardize the identification of galaxies with extreme Lyman continuum leakage. Based on our models, we expect that essentially all $z \approx 7-9$ galaxies that exhibit rest-frame EW(H β) $\lesssim 30$ Å to have $f_{\text{esc}} > 0.5$. Incorrect assumptions concerning the ionizing fluxes of stellar populations or the dust properties of $z > 6$ galaxies can in principle bias the selection, but substantial model deficiencies of this type should at the same time be evident from offsets in the observed distribution of $z > 6$ galaxies in the EW(H β)- β diagram compared to the simulated one. Such offsets would thereby allow JWST/NIRSpec measurements of these observables to serve as input for further model refinement.

Subject headings: Galaxies: high-redshift – dark ages, reionization, first stars – techniques: spectroscopic

1. INTRODUCTION

Scenarios in which star-forming galaxies provide the photons that reionize the Universe at $z > 6$ hinge on the assumption that hydrogen-ionizing (Lyman continuum, hereafter LyC) photons can readily escape from these objects and into the intergalactic medium. Current constraints place the required, time- and luminosity-averaged LyC escape fraction from galaxies in the reionization epoch at $f_{\text{esc}} \approx 0.01-0.2$ (e.g. Hartley & Ricotti 2016; Mitra et al. 2016; Sun & Furlanetto 2016; Bouwens et al. 2016), but allowing for f_{esc} evolution with mass or redshift allows for considerably higher average values

for certain subsets of reionization-epoch galaxies (e.g. Ferrara & Loeb 2013; Price et al. 2016). Simulations also predict large galaxy-to-galaxy variations in f_{esc} , with a few objects propelled to extreme levels of LyC leakage (e.g. Paardekooper et al. 2013; Yajima et al. 2014; Kimm & Cen 2014; Paardekooper et al. 2015; Cen & Kimm 2015; Xu et al. 2016).

In the local Universe, all current direct detections of escaping LyC flux indicate $f_{\text{esc}} \lesssim 0.1$ (Bergvall et al. 2006; Leitert et al. 2013; Borthakur et al. 2014; Izotov et al. 2016a; Leitherer et al. 2016; Izotov et al. 2016b), but a few objects with very high LyC escape fractions ($f_{\text{esc}} > 0.4$) have been reported at $z \approx 2-3$ (Vanzella et al. 2016; Matthee et al. 2016; Shapley et al. 2016). In general, the physical mechanisms that provide the conditions for LyC photons to escape are not well constrained. In the language of simple gas/dust geometries, LyC escape can occur either through ionization-bounded nebulae with holes (“the picket-fence” model) or through density-bounded nebulae (for detailed discussions, see Zackrisson et al. 2013; Duncan & Conselice 2015; Reddy et al. 2016). While some LyC-leaking galaxies do display the spectral signatures of density-bounded nebulae (de Barros et al. 2016), Reddy et al. (2016) argue that this scenario cannot apply to all cases.

Of course, what matters for cosmic reionization is the LyC escape fraction at $z \gtrsim 6$, where the opacity of the neutral IGM prevents the LyC to be measured directly (e.g. Inoue et al. 2014). Because of this, a number of observational methods aiming to provide indirect estimates of f_{esc} in the reionization epoch have recently been proposed (Fernandez, Dole & Iliev 2013; Jones et al. 2013; Zackrisson et al. 2013; Reddy et al. 2016; Leethochawalit et al. 2016).

Here, we continue the development of the method outlined by Zackrisson et al. (2013) to measure LyC escape

* E-mail: erik.zackrisson@physics.uu.se

¹ Department of Physics and Astronomy, Uppsala University, Box 515, SE-751 20 Uppsala, Sweden

² New Mexico State University, MSC 4500, Las Cruces, NM 88003, USA

³ Particle Astrophysics Center, Fermi National Accelerator Laboratory, Batavia, IL 60510, USA

⁴ Department of Astronomy & Astrophysics, The University of Chicago, Chicago, IL 60637 USA

⁵ Kavli Institute for Cosmological Physics and Enrico Fermi Institute, The University of Chicago, Chicago, IL 60637 USA

⁶ Universität Heidelberg, Zentrum für Astronomie, Institut für Theoretische Astrophysik, Albert-Ueberle-Str. 2, 69120 Heidelberg, Germany

⁷ Department of Earth and Space Science, Osaka University, 1-1 Machikaneyama, Toyonaka, Osaka 560-0043, Japan

⁸ College of General Education, Osaka Sangyo University, 3-1-1, Nakagaito, Daito, Osaka 574-8530, Japan

⁹ University of Michigan, Department of Astronomy, 311 West Hall, 1085 S. University Ave, Ann Arbor, MI 48109-1107 USA

¹⁰ Institute for Astronomy, University of Edinburgh, Royal Observatory, Edinburgh, EH9 3HJ, UK

¹¹ Instituto de Astrofísica de Canarias, C/ Vía Láctea s/n, E-38205 La Laguna, Tenerife, Spain

¹² Departamento de Astrofísica, Universidad de La Laguna, Av. del Astrofísico Francisco Sánchez s/n, E-38206 La Laguna, Tenerife, Spain

fractions at $z > 6$. This technique exploits the fact that f_{esc} regulates the relative impact of nebular emission on the rest-frame ultraviolet/optical spectra of high-redshift galaxies (e.g. Zackrisson, Bergvall & Leitet 2008). Using spectral features that will be observable for galaxies at $z \approx 6-9$ using the NIRSpec instrument on the upcoming James Webb Space Telescope (JWST), Zackrisson et al. (2013) argued that it should be possible to single out individual objects with very high escape fractions ($f_{\text{esc}} \gtrsim 0.5$). Unlike other methods, this technique has modest signal-to-noise and spectral resolution requirements, and can therefore be applied to large numbers of high-redshift galaxies in upcoming JWST/NIRSpec surveys.

As the work of Zackrisson et al. (2013) was based on a number of simplified assumptions concerning the properties of $z \gtrsim 6$ galaxies, we here replace the toy models used in that study with more realistic galaxies drawn from cosmological simulations. By generating mock galaxy spectra in the rest-frame ultraviolet/optical wavelength range relevant for JWST/NIRSpec, we show that neither the star formation histories nor the internal metal distributions of the simulated galaxies provide any insurmountable difficulties for the technique to identify galaxies with $f_{\text{esc}} \gtrsim 0.5$. In a separate paper, (Jensen et al. 2016) use the same mock spectra to demonstrate that it may also in principle be possible to constrain the *typical* escape fraction fraction within samples of $\gtrsim 50$ galaxies studies with JWST/NIRSpec, even if the escape fraction is not very extreme ($f_{\text{esc}} \lesssim 0.2$). The simulated spectral energy distributions (SEDs) for $z = 7-9$ galaxies with different f_{esc} , produced as part of the LYCAN (LYman Continuum ANalysis) project, are also made publicly available¹⁴.

The computational machinery and the associated assumptions used when generating the LYCAN spectra are described in Section 2. In Section 3, we discuss the impact of the star formation histories and metallicity distributions of simulated $z \approx 7-9$ galaxies on the diagnostic diagram of $H\beta$ emission-line equivalent width $\text{EW}(H\beta)$ vs. UV slope β introduced by Zackrisson et al. (2013) to identify galaxies with extreme LyC escape fractions.

While a realistic application of the proposed method to find such objects would likely involve all emission lines detectable in the rest-frame ultraviolet/optical (as in Jensen et al. 2016), the merits of focusing on this particular line is that this sidesteps many of the complexities related to the physical conditions of the gas. While several other emission lines are expected to be stronger than $H\beta$, hydrogen Balmer recombination lines¹⁵ are comparatively insensitive to gas density, metallicity and ionization parameter. Even in the case of $H\beta$, there are of course potential complications, which we discuss in Section 4. Section 5 summarizes our findings.

2. FROM COSMOLOGICAL SIMULATIONS TO SYNTHETIC GALAXY SPECTRA

2.1. Cosmological simulations of galaxy formation

In this work, four independent suites of cosmological simulations are used to capture the star formation

histories and metallicity distributions of galaxies in the reionization epoch. These are described in Finlator et al. (2013, hereafter F13), Shimizu et al. (2014, hereafter S14), Gnedin et al. (2014, *Cosmic Reionization On Computers*; hereafter CROC) and Paardekoooper et al. (2013, 2015, the *First Billion Years* simulations; hereafter FiBY).

The F13, S14 and CROC simulations provide us with large numbers of synthetic galaxies with individual variations in star formation history and metallicity distributions, plus the opportunity to check the simulation-dependence of our final SEDs. However, neither of these simulation suites directly predict the LyC escape fraction f_{esc} of individual galaxies. This is instead provided by the FiBY simulations, albeit for a much smaller number of objects in the mass range relevant for JWST observations.

While these simulations provide output at a wide range of redshifts, we will in this paper focus on galaxies selected from simulation boxes at $z \approx 7$, except in the case of FiBY simulations, for which we have selected the most massive galaxies from the $z = 6, 7$ and 8 boxes to increase the number of simulated galaxies with self-consistent f_{esc} predictions. Since the predicted evolution in galaxy properties (in terms of star formation history and internal metallicity distribution) is undramatic throughout this redshift range (see section 3.1), no significant biases are expected to arise from this approach.

Throughout most of our analysis, we also impose lower limits on the total stellar mass of the simulated galaxies for which model SEDs are generated. This mass threshold serves the purpose of excluding galaxies too faint for reliable JWST/NIRSpec measurements of $\text{EW}(H\beta)$ and β , and also to avoid artifacts related to the mass resolution of the simulations. Zackrisson et al. (2013) estimated that these JWST/NIRSpec measurements require galaxies with total stellar masses $M_{\text{stars}} \gtrsim 10^8-10^9 M_{\odot}$ in the absence of lensing and $M_{\text{stars}} \gtrsim 10^7 M_{\odot}$ in the case of strong lensing. Significant resolution issues are also expected when the total stellar mass of the simulated galaxies approaches the stellar mass resolution element (the mass of the “star particles”; see section 2.2), as this makes the retrieved star formation history too uncertain for SED modelling. In the light of this, we only consider galaxies with $M_{\text{stars}} \geq 10^7 M_{\odot}$ for F13, CROC and FiBY and $M_{\text{stars}} \geq 5 \times 10^8 M_{\odot}$ for S14. Because of differences in resolution and in the cosmological volumes used by the different simulation suites, these mass limits result in large variations in the number of objects for which LYCAN spectra are generated. At $z = 7$, our criteria yield 874 galaxies for CROC, 406 for S14 and 106 for F13. In the case of FiBY, we get no more than 16 galaxies at $M_{\text{stars}} \geq 10^7 M_{\odot}$, even when combining data from $z = 6, 7$ and 8.

In Figure 1, we show the internal metallicity distributions and star formation histories of one typical galaxy of mass $M_{\text{stars}} \sim 10^8 M_{\odot}$ at $z = 7$ from each simulation suite. While fluctuations in star formation rates (SFRs) have occurred throughout the formation of these objects, the SFRs have on average been rising since the formation of their first stars (as previously reported by e.g. Finlator et al. 2011; Jaacks et al. 2012; Shimizu et al. 2014). This is exemplified in Figure 1a, where we plot

¹⁴ LYCAN SEDs are publicly available at: <http://www.astro.uu.se/~ez/lycan/lycan.html>

¹⁵ Unfortunately, $H\alpha$ redshifts out of NIRSpec range at $z > 6.6$ – otherwise this would likely have been the best choice

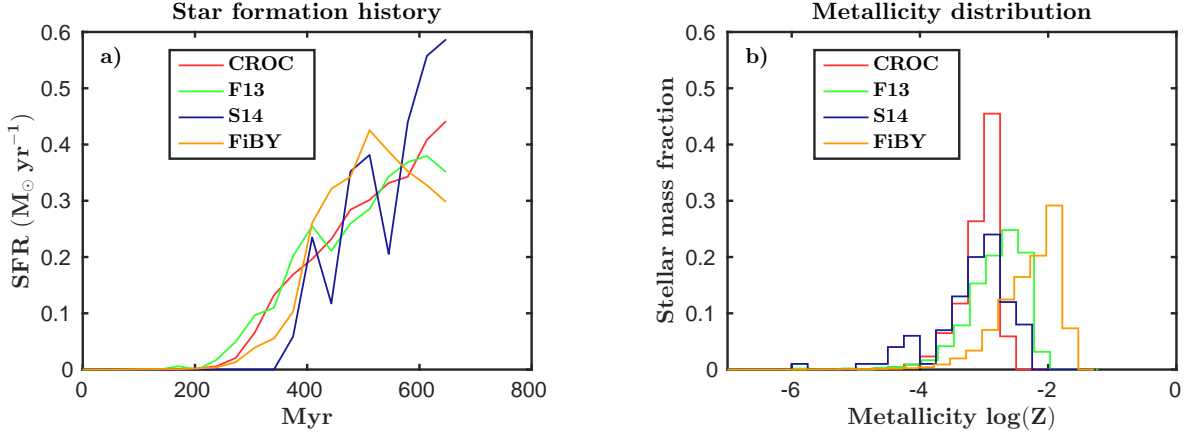


FIG. 1.— Examples of the star formation histories and internal metallicity distributions for four galaxies with $M_{\text{stars}} \sim 10^8 M_{\odot}$ at $z = 7$. The line colour represents the simulation suite from which each galaxy originates: CROC (red), F13 (green), S14 (blue) and FiBY (orange). **a)** Star formation rate as a function of time up to the age of the Universe at $z = 7$. All simulations predict a long-term trend of increasing star formation activity, but in some cases with substantial short-term fluctuations due to feedback and mergers. **b)** The stellar metallicity distribution within the four simulated galaxies. In all cases, the mass-averaged metallicity Z is below solar ($Z_{\odot} \approx 0.014$; Asplund et al. 2009), although a significant fraction of stars have attained solar and even supersolar abundances in the FiBY galaxy shown.

the SFR as a function of time for these four simulated galaxies. For plotting purposes, we have here renormalized all four objects to exactly $M_{\text{stars}} = 10^8 M_{\odot}$ to get rid of offsets due to slight differences in mass. Star formation rate fluctuations on time scales of 10–100 Myr of the type seen here (most notably in the S14 and FiBY cases) are produced by a combination of feedback effects and mergers and are commonly seen in simulations of high-redshift galaxies (e.g. Ma et al. 2015; Kimm et al. 2015).

All four suites consistently predict the metallicity distribution within a single $M_{\text{stars}} \sim 10^8 M_{\odot}$ galaxy at $z = 7$ to be wide (varying by ≈ 2 dex) and to have a mass-weighted average $Z < Z_{\odot}$. Only a very small fraction of stars (always $< 10\%$ and typically much fewer) are predicted to be in the extremely metal-poor range ($Z < 10^{-5}$) where the IMF is suspected to become top-heavy (e.g. Dopcke et al. 2013; Safranek-Shrader et al. 2014). There are, however, substantial systematic differences in average metallicity between the simulations, as exemplified in Figure 1b – with CROC typically predicting the lowest mean metallicities and FiBY the highest. At $M_{\text{stars}} \sim 10^8 M_{\odot}$, the mean metallicity varies from $Z \approx 10^{-3}$ (i.e. $\sim 0.1 Z_{\odot}$) to $Z \approx 10^{-2}$ (only slightly subsolar) between the simulation suites. However, these metallicity variations do not have any significant impacts on the results in this paper, as demonstrated in Section 3.1.

2.2. SED modelling

2.2.1. Stellar and nebular contributions to the SED

The internal stellar age and metallicity distribution from each simulated galaxy is stored as a collection of star particles (mass $\sim 10^3$ – $10^6 M_{\odot}$ depending on simulation resolution), each considered to have a single age and metallicity. By using the Yggdrasil spectral synthesis code (Zackrisson et al. 2011) to attach a suitable model spectral energy distribution (SED) to each such star particle and summing over all star particles belonging to specific galaxy, the complete SED of that galaxy is generated. The end product is an SED in the rest-frame 0.1216–1 μm wavelength range (relevant

for JWST/NIRSpec observations of $z > 6$ galaxies) that takes both starlight, nebular emission (nebular emission lines plus nebular free-bound and free-free continuum), dust attenuation and LyC leakage into account.

The first step of this procedure is to generate a stellar SED suitable for each star particle from a pre-generated grid of single stellar population (SSP) models covering a wide range in age t and metallicity Z . Here, we have chosen to interpolate this grid in $\log(t)$ and $\log(Z)$ to produce this star particle SED. Tests with alternative computational schemes (interpolation in linear t and Z or by simply picking the closest grid SSP model) indicate that the end results are not particularly sensitive to how this interpolation is carried out.

To evaluate the impact of different assumptions concerning stellar evolution, a number of alternative SSP grids have been used. The one we consider as the default option in this paper consists of Starburst99 (Leitherer et al. 1999) SSP stellar population spectra based on Geneva tracks with high mass-loss and no rotation at $Z = 0.001$ – 0.040 , extended to lower metallicities with Raiter et al. (2010) SSP models at $Z = 10^{-5}$ and $Z = 10^{-7}$. All models have been scaled to match the Kroupa (2001) universal stellar initial mass function (IMF).

This assumption of an invariant IMF can certainly be questioned at metallicities close to the Population III regime ($Z \sim 10^{-5}$, 10^{-7} in our grid), where the IMF is expected to turn top-heavy. However, as discussed in section 2.1 and 3.1, this choice has a very small impact on the majority of galaxies in our simulations, since very few star particles tend to have metallicities in this range.

As alternatives to our baseline grid, we also consider versions for which the Starburst99 Geneva models have been replaced by Starburst99 Padova-AGB models (Vázquez & Leitherer 2005) at $Z = 0.0004$ – 0.050 or by BPASS v.2.0 models (Stanway et al. 2016) for binary stars at $Z = 0.001$ – 0.030 .

For each stellar population SSP grid, nebular spectra for different LyC escape fractions f_{esc} have also been generated using the photoionization code Cloudy (Ferland et al. 2013), based on the assumption of spheri-

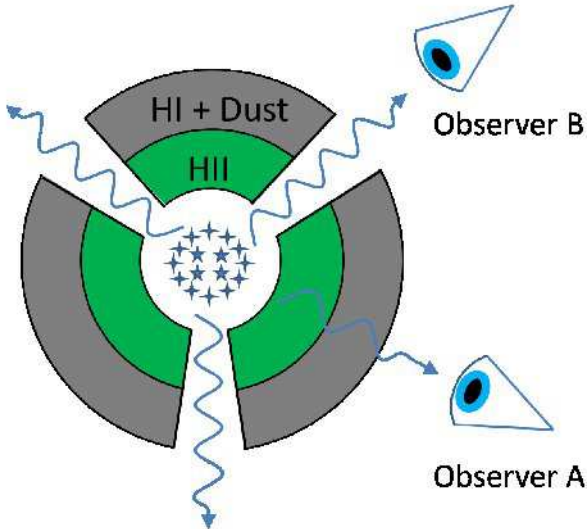


FIG. 2.— Schematic illustration of the two different viewing angles considered when simulating the impact of dust attenuation on observed galaxy SEDs. The galaxy is here assumed to consist of a central star-forming region, a surrounding photoionized region (green) and an outer shell of neutral gas and dust (grey). Observer A happens to be viewing the galaxy from an angle which does not include any direct starlight. Since observer A receives nebular emission from the whole photoionized region, the relative impact of nebular emission on the galaxy SED observed by A drops with increasing LyC escape fraction f_{esc} . However, the impact of dust attenuation on this SED does not necessarily weaken with increasing f_{esc} since all the light received by A passes through dusty regions (grey). The galaxy SED seen by observer B, on the other hand, contains a fraction of direct, unattenuated starlight.

cal, constant-density nebulae ($n(\text{H}) = 100 \text{ cm}^{-3}$) with the same metallicity as that of the stars. Within these nebulae, the electron temperature responds self-consistently to changes in the ionizing SED (see Zackrisson et al. 2011, 2013, for further details).

As discussed in Zackrisson et al. (2013), LyC leakage can take place through two basic scenarios – leakage through a radiation-bounded nebula with holes or leakage through a density-bounded nebula. As demonstrated in that paper, the two mechanisms give rise to similar predictions in the $\text{EW}(\text{H}\beta)$ - β diagram in the dust-free case. Things get more complicated when dust effects are considered, since the direct absorption of Lyman continuum photons of dust (see section 4.1) is likely to be more important in the density-bounded case. In this paper, we for simplicity focus on the case of radiation-bounded nebulae with holes free of both gas and dust. In this case, the LyC escape fraction is simply regulated by the gas covering fraction f_{cov} adopted in Cloudy ($f_{\text{esc}} = 1 - f_{\text{cov}}$). Since a number of recent observations (see section 4.3) indicate that density-bounded nebula may also be highly relevant, we are planning a follow-up paper dedicated to this specific mode of LyC escape.

2.2.2. Dust attenuation

To account for the effects of dust in the rest-frame UV/optical, we consider two alternative recipes developed by F13 and S14 for predicting the attenuation of simulated galaxies. In the F13 recipe, the rest-frame color excess $E(B-V)$ is based on a deterministic part related to the overall stellar population metallicity Z , plus

a random component $\delta E(B-V)$:

$$E(B-V) = 9.0Z^{0.9} + \delta E, \quad (1)$$

where δE is a Gaussian component with a variance equal to half of the metallicity-dependent component. In the case of our $z = 7$ sample of galaxies from the Finlator et al. (2013) simulations, this gives an average $E(B-V) \approx 0.026$, which converts into average $\langle A(V) \rangle \approx 0.1$ – 0.2 magnitudes (where the exact value depends on the attenuation law; see below).

The S14 recipe is based on the metallicity, total stellar mass and the spatial distribution of stars within each galaxy, with free model parameters calibrated against the rest-frame UV luminosity function at $z = 7$ (for details, see Shimizu et al. 2014). The end result is a prediction of the 1500 Å attenuation ($A(1500)$) for each galaxy, which converts into an average optical extinction that is somewhat higher than for the F13 case, with $\langle A(V) \rangle \approx 0.2$ – 0.4 depending on the attenuation law.

Once either $E(B-V)$ – the Finlator case – or $A(1500)$ – the Shimizu case – has been established, we consider a number of different wavelength-dependent dust attenuation laws to apply reddening throughout the full wavelength range of our model SEDs: the LMC and SMC attenuation laws by Pei (1992) or the Calzetti et al. (2000) attenuation law for starburst galaxies. In the case of the LMC and SMC attenuation laws, we assume the attenuation to affect the stellar and nebular portions of the SED by an equal factor. In the Calzetti et al. (2000) case, we allow the reddening of the stellar component either to be equal to that of the nebular one ($E(B-V)_{\text{stars}} = E(B-V)_{\text{neb}}$), or a factor of 0.44 lower ($E(B-V)_{\text{stars}} = 0.44E(B-V)_{\text{neb}}$, i.e. the case actually advocated by Calzetti et al. 2000). The higher $E(B-V)$ implied for the nebular component in the latter case is usually interpreted as an effect of age-dependent attenuation, in the sense that young star-forming regions are embedded within thick dust cocoons that disperse over time (Charlot & Fall 2000; Bergvall et al. 2016). One would then expect the $f = E(B-V)_{\text{neb}}/E(B-V)_{\text{stars}}$ ratio to depend on star formation history, effectively approaching unity in cases where all stars have the same age or when young star-forming regions come to dominate the spectrum. Indeed, observational studies support this, indicating that f depends on the specific star formation rate (e.g. Price et al. 2014; Puglisi et al. 2016). To capture this variation in f across a sample of simulated galaxies, it would seem more realistic to apply age-dependent attenuation corrections to each star particle separately, rather than relying on galaxy-wide attenuation corrections. However, tests using the age-dependent dust attenuation recipe developed by Bergvall et al. (2016) – with parameters tuned to make the average UV slope β of the $z = 7$ galaxy population agree with observations – applied to each star particle indicates that this produces results that are qualitatively similar to the $E(B-V)_{\text{stars}} = 0.44E(B-V)_{\text{neb}}$ case in the $\text{EW}(\text{H}\beta)$ - β diagram. Throughout the rest of this paper, we will therefore consider galaxy-wide attenuation corrections only.

The effect of dust reddening on the observed SED may potentially be reduced in the case of very high f_{esc} , but the impact of this effect is likely to depend on the geome-

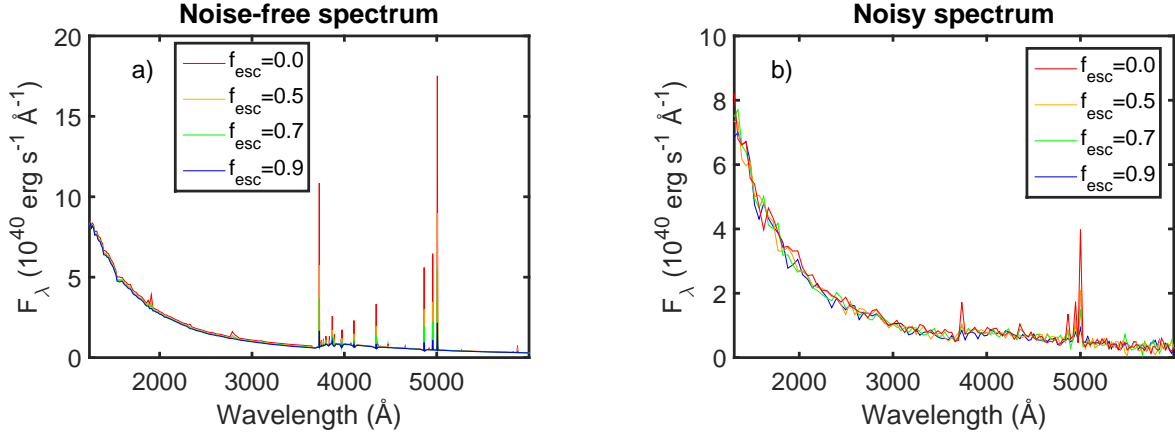


FIG. 3.— Synthetic spectra of a single $M_{\text{stars}} \approx 7 \times 10^8 M_{\odot}$, $m_{\text{AB}} \approx 27$, dust-free Shimizu et al. (2014) galaxy for different f_{esc} : 0.0 (red), 0.3 (orange), 0.5 (green) and 0.7 (blue). **a)** Noiseless spectra **b)** Spectra degraded to the spectral resolution of the JWST/NIRSpec $R = 100$ prism, and with noise level corresponding to a 10 h exposure. The f_{esc} parameter mainly affects the strength of the emission lines relative to the continuum, and this effect remains detectable for the strongest emission lines (here $[\text{OII}]\lambda 3727$, $\text{H}\beta$, $[\text{OIII}]\lambda 4959$ and $[\text{OIII}]\lambda 5007$) even after the introduction of observational noise. In Figure 4, we also show a zoom-in on the region around the latter three lines.

try of gas, stars and dust, the level of leakage isotropy and the viewing angle of the observer. This is schematically illustrated in Figure 2, where two observers A and B are viewing an ionization-bounded nebula with holes from different angles. Observer A measures an SED where all the starlight and nebular emission has passed through a dust screen, which – at least to first order – may be considered to be unaffected by f_{esc} (this is hereafter referred to as scenario A). Observer B, on the other hand, measures an SED which contains a fraction of unattenuated starlight. In the case of highly isotropic leakage through many thin escape channels, a fraction f_{esc} of the starlight directed towards observer B may be unaffected by dust whereas a fraction $1 - f_{\text{esc}}$ experiences dust attenuation (hereafter scenario B). However, these are admittedly not the only options, since anisotropic leakage could allow a fraction of unattenuated starlight different from the global f_{esc} to escape in the direction of B. Throughout this paper, we consider scenario A the default option, but also explore the consequences of scenario B on the $\text{EW}(\text{H}\beta)$ - β diagram.

2.2.3. Simulating JWST/NIRSpec data quality

To provide realistic simulations of galaxy spectra as they would appear when observed with the JWST/NIRSpec instrument, our model also allows the option of degrading the quality of the simulated SEDs by taking the noise and limited spectral resolution into account, following the JWST/NIRSpec-specific recipe described in Jensen et al. (2016).

As an example of how f_{esc} affects the SED in the wavelength range relevant for JWST/NIRSpec, we in Figure 3 show the predicted SED of a dust-free, $M_{\text{stars}} \approx 7 \times 10^8 M_{\odot}$ galaxy from the Shimizu et al. (2014) batch at $z = 7$ for various f_{esc} , with and without instrumental effects (noise and degraded spectral resolution). At this redshift, this object attains an apparent magnitude of $m_{\text{AB}} \approx 27$ in the rest-frame ultraviolet, where the SED is continuum dominated.

Here, we have assumed a very long exposure time ($t_{\text{exp}} = 10$ h) using the $R = 100$ NIRSpec prism. As argued by Zackrisson et al. (2013), f_{esc} mainly affects the strengths of emission lines compared to the continuum,

and while observational effects will render the weaker emission lines impossible to detect, several strong emission lines remain potentially useful as LyC leakage diagnostics, including $[\text{OII}]\lambda 3727$, $\text{H}\gamma$, $\text{H}\beta$, $[\text{OIII}]\lambda 4959$ and $[\text{OIII}]\lambda 5007$. While the $[\text{OII}]\lambda 3727$ and $[\text{OIII}]\lambda 5007$ emission lines actually appear as the strongest lines in the SED, the relative strengths of these lines are sensitive to the mechanism of LyC leakage, and may be very different in case of a density-bounded nebula compared to the matter-bounded nebula with holes assumed here. Following Zackrisson et al. (2013), we hence focus on the diagnostic properties of the Balmer line $\text{H}\beta$ (4863 Å; the third strongest line in the SED plotted), as the predictions for this line are very similar in the two cases. The $\text{H}\beta$ line is also convenient because the physics of hydrogen recombination is relatively simple at densities typical of the interstellar medium in galaxies – in the absence of LyC leakage, the $\text{H}\beta$ luminosity is not significantly affected by the gas density, the ionization parameter or the gas metallicity. Hence, there is no significant difference between models where the whole stellar population is considered to be a central light source surrounded by nebular gas (as assumed here and illustrated in Figure 2), or whether the stars and gas are mixed. This is in stark contrast to the behaviour of other potentially useful lines like $\text{CIII}]\lambda 1909$, $\text{CIV}\lambda 1549$, $[\text{OII}]\lambda 3727$, $[\text{OIII}]\lambda 4959$ and $[\text{OIII}]\lambda 5007$, which are more sensitive to the physical state of the nebula (e.g. Nakajima & Ouchi 2014; Stasinska et al. 2015; Jaskot & Ravindranath 2016).

In Fig. 4, we present a zoom-in of the SEDs from Fig. 3b to illustrate the expected data quality in the wavelength range surrounding the $\text{H}\beta$ line. As seen, the $\text{H}\beta$ line becomes challenging to detect at $f_{\text{esc}} \gtrsim 0.5$, but as long as its expected position can be inferred from the wavelengths of the stronger $[\text{OIII}]\lambda 4959$ and $[\text{OIII}]\lambda 5007$ lines, it should still be able to set an upper limit on $\text{EW}(\text{H}\beta)$, which is quite sufficient to single out galaxies with very high levels of LyC leakage and set a lower limit on f_{esc} . At $f_{\text{esc}} \gtrsim 0.9$, however, all of these lines become difficult to detect, which makes for substantial uncertainties in determining the redshift, unless this can be done from the detection of the Lyman- α break

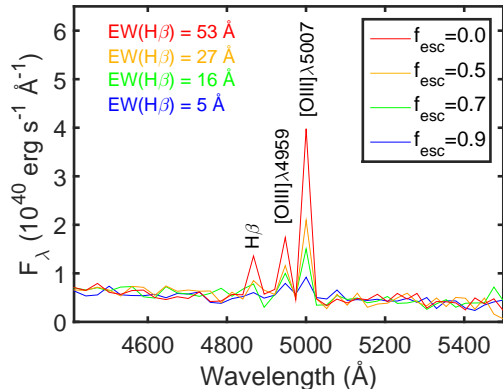


FIG. 4.— The rest-frame wavelength interval around $H\beta$, $[OIII]\lambda 4959$ and $[OIII]\lambda 5007$ extracted from the noisy, Shimizu et al. (2014) SEDs ($m_{AB} \approx 27$, $t_{exp} = 10$ h, $R = 100$) of Fig. 3b. The rest-frame $EW(H\beta)$ for this particular galaxy are listed for f_{esc} : 0.0 (red), 0.5 (orange), 0.7 (green) and 0.9 (blue). As seen, low $EW(H\beta)$ serves as a tell-tale signature of high- f_{esc} , and although a robust detection of the $H\beta$ emission line will be very challenging at $f_{esc} > 0.5$, an upper limit on $EW(H\beta)$ can still be imposed as long as the expected position of $H\beta$ is known from the redshift measured from the stronger $[OIII]\lambda 4959$ and $[OIII]\lambda 5007$ lines.

(as in Oesch et al. 2016).

3. THE $EW(H\beta)$ - β DIAGRAM

3.1. The case without dust attenuation

In Figure 5, we show the behavior of dust-free galaxies with various f_{esc} from the S14, CROC, F13 and FiBY simulation suites in the $EW(H\beta)$ - β diagram. Here, β (defined as $f_\lambda \propto \lambda^\beta$) is derived from the ten wavelength intervals in the rest-frame range ≈ 1270 -2580 Å defined by Calzetti et al. (1994). All SEDs are here based on Geneva stellar evolutionary tracks. In the case of the first three simulation suites, we explore the effects of $f_{esc} = 0$ (red dots), 0.5 (orange), 0.7 (green) and 0.9 (blue), whereas f_{esc} is self-consistently predicted in the case of the FiBY galaxies. The latter objects have been color-coded to match the f_{esc} bins that they are deemed to fall closest to (most at $f_{esc} = 0$ but a few at $f_{esc} = 0.9$).

While galaxy-to-galaxy variations in star formation history and metallicity distributions induces a considerable scatter in $EW(H\beta)$ - β space, the different f_{esc} models still produce relatively well-separated regions in this diagram. This suggests that the method proposed by Zackrisson et al. (2013) to identify high- f_{esc} galaxies is relatively robust to uncertainties regarding the ages and metallicity stellar populations of galaxies at these redshifts, at least in the absence of dust attenuation. In Figure 5d, we compare the predicted distribution of objects in the $EW(H\beta)$ - β diagram for 100 randomly-selected CROC galaxies at $z = 7$ and $z = 9$. While $z = 9$ galaxies have slightly bluer β and higher $EW(H\beta)$ due to their somewhat lower ages, the evolution between these redshifts is marginal, which means that our $z = 7$ results should apply to the whole $z = 7$ -9 interval.

The regions spanned by different f_{esc} are also relatively consistent among the four simulations used. However, since the simulations display different galaxy-to-galaxy diversity in star formation history and metallicity distribution, the compactness of the regions differ. For instance, the CROC galaxies exhibit smaller and more

well-defined regions than the others, mainly due to their smoother star formation histories.

3.2. Uncertainties related to stellar evolution

While the diagnostic value of the $EW(H\beta)$ - β diagram in identifying high- f_{esc} galaxies appears relatively robust to variations in star formation history and metallicity (at least at the level of variation seen in the four simulation suites explored), there are other model uncertainties that could potentially bias the outcome. Any stellar population property that substantially boosts the ionizing stellar ultraviolet continuum compared to the non-ionizing ultraviolet continuum flux would result in a bias of the f_{esc} inferred from observations, if not accounted for in the models.

A generic prediction when approaching the population III metallicity regime ($Z \lesssim 10^{-5}$) is a boost in the characteristic mass of stars (e.g. Dopcke et al. 2013; Safranek-Shrader et al. 2014). As demonstrated by Zackrisson et al. (2013), this would have a very pronounced impact on the $EW(H\beta)$ - β diagram by pushing objects upwards (towards redder β slopes) through a boost in the relative impact of nebular emission at fixed f_{esc} . While our simulations predict mean metallicities $Z > 10^{-4}$ for all galaxies sufficiently massive to be within range of NIRSpec at $z > 6$, there is a minority of star particles with metallicities ranging from $Z = 0$ to $Z \sim 10^{-5}$ in these objects, for which the choice of the Kroupa (2001) IMF could certainly be questioned. However, for this to have any significant effect on the total SED also requires that these galaxies are caught in the phase where these particular star particles are younger than a few Myr. This condition is never met by more than $\approx 1\%$ of the star particles in any of our simulated galaxies and there is consequently no outliers predicted at very red β and very high $EW(H\beta)$ in Figure 5, even if the extremely top-heavy Population III IMF considered by Zackrisson et al. (2013) is applied to the $Z < 10^{-5}$ particles. We therefore conclude that the assumptions on the behavior of the IMF at very low metallicities is not a major hurdle for our method to measure f_{esc} .

Uncertainties in the treatment of stellar evolution at higher metallicities can also be important, and recent studies have highlighted that both stellar rotation (e.g. Levesque et al. 2012; Leitherer et al. 2014; Topping & Shull 2015) and binary evolution (e.g. Eldridge & Stanway 2009; Stanway et al. 2016; Wilkins et al. 2016; Ma et al. 2016) may affect the ionizing fluxes of stellar populations by factors of a few. Since model grids that treat such effects have yet to be released for the full range of metallicities seen in our simulated galaxies, a completely self-consistent test of such effects is beyond the scope of the present study. However, since the fraction of star particles at metallicities $Z < 10^{-4}$ is low, an assessment of the likely effects can nonetheless be made by exchanging the model grids at higher metallicities for those based on assumption different from those in our default batch. In Figure 6a, we demonstrate the effects of switching from SB99 models based on Geneva stellar evolutionary tracks to Padova stellar evolutionary tracks in the case of the S14 galaxies. This turns out to have a very modest impact on the predicted position of galaxies in the $EW(H\beta)$ - β diagram, and would not bias f_{esc} estimates in any significant way.

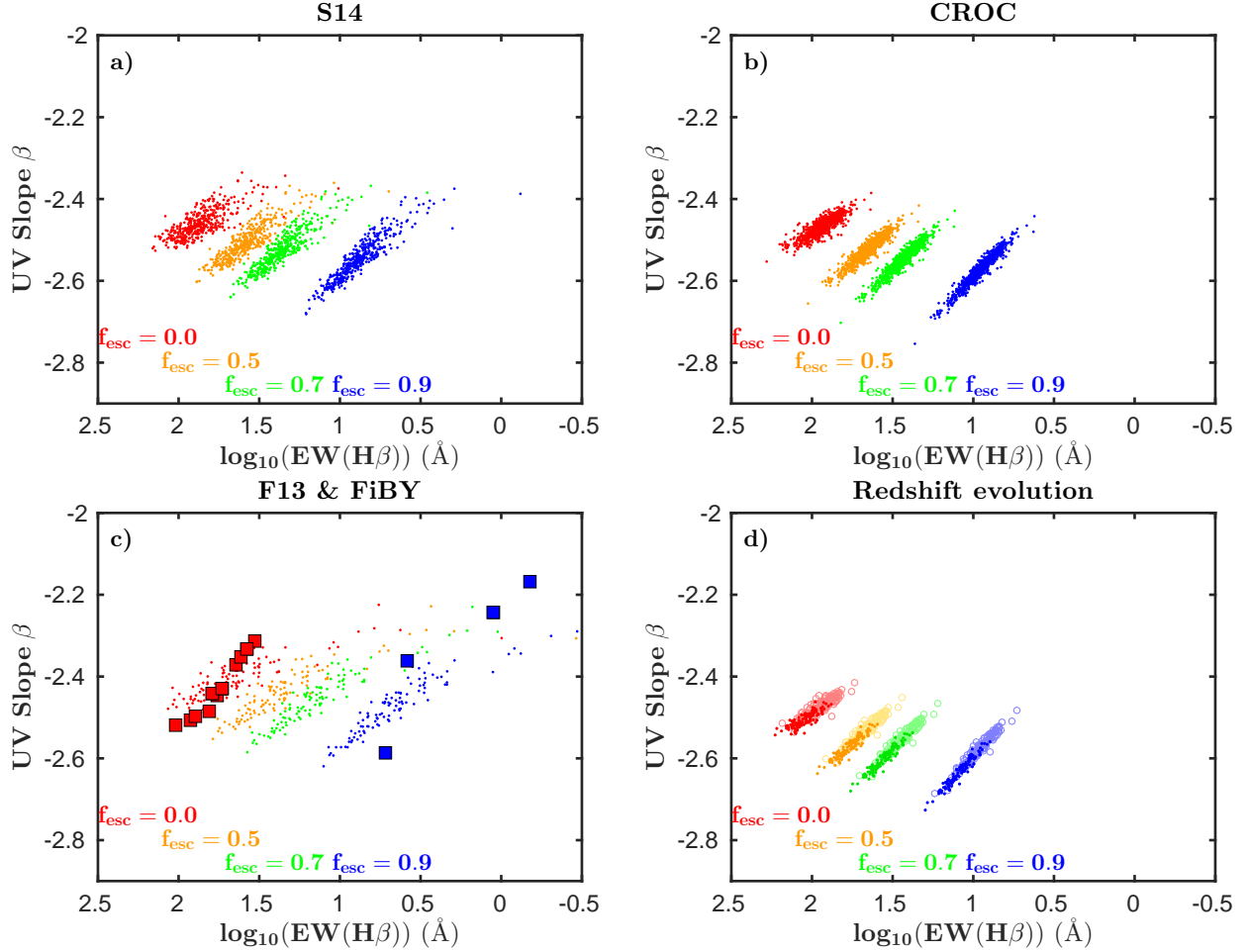


FIG. 5.— The position of synthetic, dust-free galaxies in the $\text{EW}(\text{H}\beta)$ - β diagram for escape fractions $f_{\text{esc}} = 0.9$ (blue markers), 0.7 (green), 0.5 (orange) and 0.0 (red). **a)** Galaxies at $z = 7$ from Shimizu et al. (2014); **b)** Galaxies at $z = 7$ from CROC; **c)** Galaxies at $z = 7$ from Finlator et al. (2013) and at $z = 6-8$ from the FiBY simulations (squares). Please note that the LyC escape fractions in the Shimizu et al. (2014), CROC and Finlator et al. (2013) simulations are *assumed*, whereas they are *predicted* in the case of FiBY, and colored according to their approximate f_{esc} . **d)** Comparison of the positions of 100 randomly selected CROC galaxies with $M_{\text{stars}} \geq 10^7 M_{\odot}$ at $z = 9$ (dark dots) and $z = 7$ (light circles). Only modest evolution in the $\text{EW}(\text{H}\beta)$ and β distributions is seen between these redshifts.

A more dramatic effect is seen in Figure 6b, where we show the effect of making a corresponding switch from SB99 Geneva models for single stars to BPASS models for binary stars. In this case, both the $\text{EW}(\text{H}\beta)$ and β distributions of the galaxy population are shifted, by as much as $\Delta \log_{10} \text{EW}(\text{H}\beta) \approx 0.5$ (i.e. a factor of ≈ 3 shift in $\text{EW}(\text{H}\beta)$) and by $\Delta \beta \approx 0.15$.

However, it should be possible to probe the observational data for signs of mismatches between the stellar evolution assumptions adopted in the simulations and the stellar evolution taking place in real galaxies, and thereby calibrate the models before attempting to infer f_{esc} . Such calibrations can either be done at low redshifts, by simply testing models based on different assumptions concerning stellar rotation and binarity against local stellar populations (e.g. Wofford et al. 2016), or directly from JWST/NIRSpec observations of galaxies at $z > 6$. As seen in Figure 6b, because of the higher ionizing fluxes produced once binary stars are considered, BPASS predicts the presence of galaxies with $\log_{10} \text{EW}(\text{H}\beta) > 2$ galaxies at $z = 7$ that are not predicted to exist in the case of models without binary evolution. Hence, the detection of a substantial number of

objects with such properties would clearly invalidate our default models based on the evolution of single stars.

3.3. Dust effects

At low levels of LyC leakage, the different dust attenuation recipes described in Section 2.2 give rise to mean optical (rest-frame V-band) attenuation values of $A_V \approx 0.15-0.4$ mag, depending on the dust attenuation curve adopted, which leads to average UV β slopes of $\beta \approx -2.2$ to -2.0 , in rough agreement with current observations of $z \approx 7$ galaxies (e.g. Bouwens et al. 2014).

Since both the $\text{H}\beta$ and $\text{H}\gamma$ emission lines are detectable with JWST/NIRSpec at $z = 6-9$, and since the intrinsic line ratio is well-constrained from recombination theory, Zackrisson et al. (2013) suggested that these lines could be used to correct NIRSpec spectra for dust reddening at these redshifts. However, we find that the modest optical dust attenuation combined with the relatively weak $\text{H}\gamma$ line (rest-frame equivalent width $\lesssim 10 \text{ \AA}$ in the case of $f_{\text{esc}} = 0$ and even weaker for higher f_{esc}) predicted for our simulated galaxies will in most cases make it practically impossible to apply any sensible dust corrections this way. Machine learning methods that exploit the

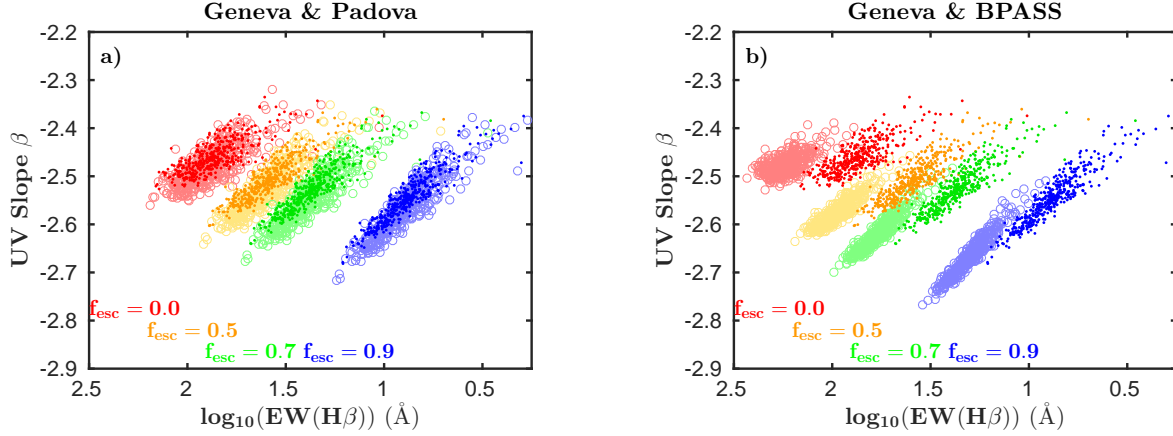


FIG. 6.— The positions of dust-free galaxies at $z = 7$ from the Shimizu et al. (2014) simulations in the $\text{EW}(\text{H}\beta)$ - β diagram, under different assumptions concerning stellar evolution. The different colors represent LyC escape fractions $f_{\text{esc}} = 0.9$ (blue), 0.7 (green), 0.5 (orange) and 0.0 (red). **a)** SEDs based on SB99 Geneva stellar evolutionary tracks (dark dots) compared to SB99 Padova stellar evolutionary tracks (light circles); **b)** SEDs based on SB99 Geneva stellar evolutionary tracks (dark dots) compared to BPASS stellar models with binary evolution (light circles). While the difference in predictions based on Geneva and Padova tracks are minor, binary evolution (as implemented in the BPASS models) leads to substantial differences, which will inevitably introduce a bias in the f_{esc} inferred from observational data unless accounted for in the models. However, it should be possible to use the overall distribution of galaxies in the $\text{EW}(\text{H}\beta)$ - β diagram to test for model deficiencies of this type.

combined marginal detections of several weak spectral features (e.g. $\text{H}\gamma$, $\text{H}\delta$, $\text{H}\epsilon$...) may still be able to provide some handle on the dust reddening, although with substantial uncertainties (Jensen et al. 2016).

Figure 7 illustrates the effect of dust on the $\text{EW}(\text{H}\beta)$ - β diagram for galaxies where the viewing angle corresponds to scenario A (i.e. f_{esc} -independent attenuation). The different panels show the behavior of S14 galaxies subject to the LMC, SMC, Calzetti $E(B-V)_{\text{stars}} = E(B-V)_{\text{neb}}$ and Calzetti $E(B-V)_{\text{stars}} = 0.44E(B-V)_{\text{neb}}$ attenuation laws. The behavior of galaxies from the other simulation suites subject to the Finlator dust recipe is very similar. The effects of the LMC, SMC and Calzetti $E(B-V)_{\text{stars}} = E(B-V)_{\text{neb}}$ attenuation laws (Figure 7abd) is to significantly reduce the usefulness of the β slope as a diagnostic of LyC leakage, since β becomes dominated by dust effects rather than the recent star formation history. Because of this, the β distribution becomes very similar for all f_{esc} considered, and $\text{EW}(\text{H}\beta)$ may by itself then be used to gauge f_{esc} . The situation is, however, quite different for the Calzetti $E(B-V)_{\text{stars}} = 0.44E(B-V)_{\text{neb}}$ case (Figure 7c), since dust attenuation in this case not only affects β , but simultaneously also decreases $\text{EW}(\text{H}\beta)$ by diminishing the relative impact of nebular emission in the spectrum. Galaxies therefore form diagonal distributions in the $\text{EW}(\text{H}\beta)$ - β diagram, qualitatively similar to the dust-free case depicted in Figure 5 but extending to redder β .

Inferring f_{esc} from the position of a single galaxy in the $\text{EW}(\text{H}\beta)$ - β diagram would lead to significant degeneracies without any knowledge on the effective attenuation law. As an example, consider the position of a galaxy at $\beta \approx -2$ and $\log_{10} \text{EW}(\text{H}\beta) \approx 1.5$. In the LMC, SMC and Calzetti $E(B-V)_{\text{stars}} = E(B-V)_{\text{neb}}$ cases, the LyC leakage would be inferred to be $f_{\text{esc}} \approx 0.5$ – 0.7 , whereas in the $E(B-V)_{\text{stars}} = 0.44E(B-V)_{\text{neb}}$ case, one would infer $f_{\text{esc}} \approx 0$ – 0.5 . Information on the effective attenuation law from observations at slightly lower redshifts may help guide the analysis, and so may the distribution of objects at $z > 6$ in the $\text{EW}(\text{H}\beta)$ - β diagram itself (similarly to the situation discussion in section 3.2), but a

case in which the effective attenuation law changes from galaxy to galaxy at $z > 6$ would inevitably lead to a very problematic situation.

Figure 8 illustrates the effect of dust on the $\text{EW}(\text{H}\beta)$ - β diagram in the alternative scenario B (where unattenuated starlight escapes along the line of sight, leading to f_{esc} -dependent dust attenuation) for an LMC attenuation law. At $f_{\text{esc}} = 0$ (not shown), scenario B gives predictions identical to those of scenario A in Figure 7, but at higher f_{esc} , scenario B produces SEDs with β slopes that are more similar to the completely dust-free case in Figure 5. Hence, the β slope can in this scenario appear very blue even though there is substantial dust attenuation in the galaxy. This happens because the unattenuated fraction f_{esc} of the starlight (which give very blue β) comes to dominate the rest-frame UV continuum and hence the overall β slope. At $f_{\text{esc}} > 0.5$, the predicted distribution of β slopes is only marginally different from the dust-free case (here shown as symbols in a darker shade). The $\text{EW}(\text{H}\beta)$ distribution at these very high f_{esc} is, on the other hand, expected to be shifted to $\text{EW}(\text{H}\beta)$ slightly lower than in the dust-free case due to a boost in the overall $\text{H}\beta$ continuum from the direct, unattenuated starlight. While it would in many cases be impossible to observationally determine which of the scenarios A and B is the most relevant, this is not necessarily a problem for identifying galaxies with very high levels of LyC leakage ($f_{\text{esc}} > 0.5$), since these would exhibit very low $\text{EW}(\text{H}\beta)$ in both cases. There is, however, one special case where the observables we consider would favour one geometry over the other: Since scenario B galaxies with very high f_{esc} always exhibit blue β slopes ($\beta < -2.2$), the detection of a galaxy with very low $\text{EW}(\text{H}\beta)$ and a red β ($\beta > -2.2$) would suggest that the viewing angle is more similar to scenario A.

4. DISCUSSION

In previous sections, we have demonstrated that indirect spectral signatures of LyC leakage in the rest-frame ultraviolet and optical should be readily detectable with JWST/NIRSpec at $z = 7$ – 9 , and that individual galaxies

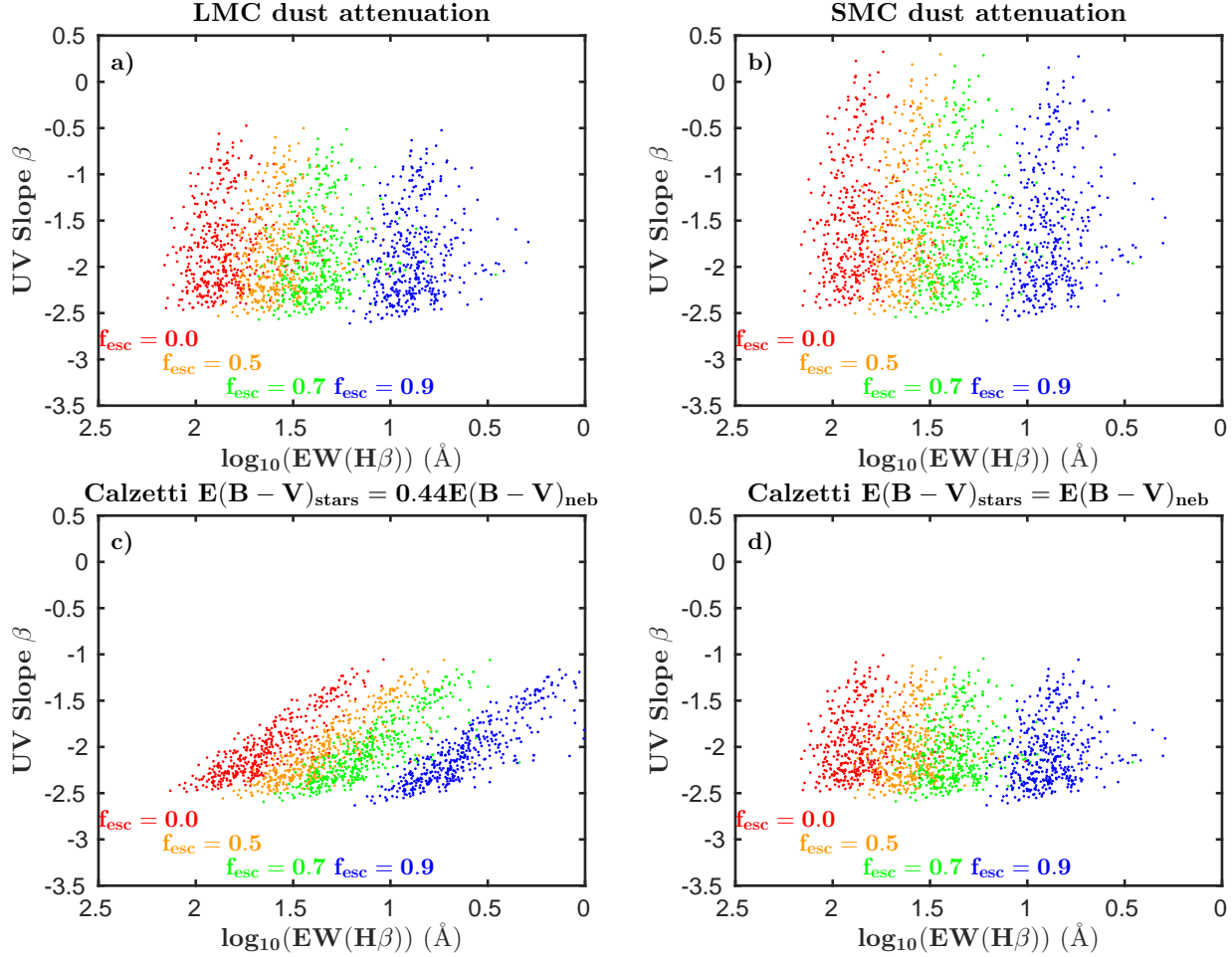


FIG. 7.— Effects of dust attenuation on $M_{\text{stars}} \geq 5 \times 10^8 M_{\odot}$ galaxies at $z = 7$ from the Shimizu et al. (2014) simulations in the $\text{EW}(\text{H}\beta)$ - β diagram under the assumption of orientation scenario A. The different colors represent LyC escape fractions $f_{\text{esc}} = 0.9$ (blue), 0.7 (green), 0.5 (orange) and 0.0 (red). **a)** Galaxies obeying the LMC attenuation law **b)** SMC attenuation law **c)** Calzetti attenuation law with $E(B - V)_{\text{stars}} = 0.44E(B - V)_{\text{neb}}$ **d)** Calzetti $E(B - V)_{\text{stars}} = E(B - V)_{\text{neb}}$

with very high LyC escape fractions ($f_{\text{esc}} \geq 0.5$) should be identifiable at these redshifts based on their position in the β vs $\text{EW}(\text{H}\beta)$ diagram. In a companion paper (Jensen et al. 2016), we also show that the full range of spectral information available from JWST/NIRSpec, low-resolution spectra should allow for constraints with a mean statistical error of $\Delta f_{\text{esc}} \approx 0.1$. This method of using continuum and emission-line data to constrain LyC leakage from reionization-epoch galaxies has the obvious advantage over competing methods based on absorption lines (Jones et al. 2013; Reddy et al. 2016; Leethochawalit et al. 2016) of not requiring high spectral resolution or as high signal-to-noise ratios, which means that it can be applied to much larger samples of $z > 6$ galaxies. A recent attempt to test the metal absorption line method using direct LyC measurements at $z \approx 2.4$ also failed to verify the predicted LyC flux (Vasei et al. 2016), indicating potential problems with this approach. One can, however, envision similar problems with our proposed method as well. In the following, we will discuss a number of potential pitfalls that require further consideration.

4.1. Lyman continuum attenuation by dust

As pointed out by Zackrisson et al. (2013), the method of using the relative strength of emission lines to assess f_{esc} would overestimate f_{esc} in cases where some non-negligible fraction of the LyC photons that do not escape is directly absorbed by dust rather than gas. For instance, the models presented by Cai et al. (2014) suggest that dust attenuation may reduce the fraction of ionizing photons captured by gas by a factor of ≈ 2 even at $z \approx 6-9$. In terms of the classical geometries often used in photoionization modelling, LyC attenuation by dust occurs in density-bounded nebulae with an outer dust shell, and in both ionization-bounded and density-bounded nebulae when photoionized gas and dust are mixed (see Figure 8 in Zackrisson et al. 2013). LyC attenuation by dust can also happen if dust is sprinkled within the escape channels of an ionization-bounded nebula with holes, although the simulations of Gnedin et al. (2008) indicate that when LyC escapes, it tends to do so through dust-free channels.

Observations of the rest-frame far-IR continuum from dust emission can constrain the level of LyC extinction (Inoue 2001; Inoue et al. 2000, 2001b; Hirashita et al. 2003) and the study by Borthakur et al. (2014) suggests that this mechanism may have a substantial impact on f_{esc} for LyC-leaking galaxies at low redshift. However, at

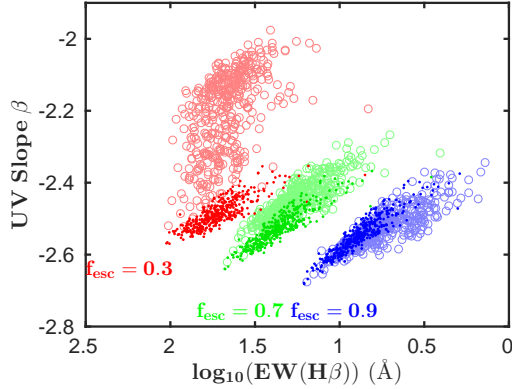


FIG. 8.— Effects of dust attenuation on $z = 7$ galaxies from the Shimizu et al. (2014) simulations in the $\text{EW}(\text{H}\beta)$ - β diagram under the assumption of orientation scenario B (f_{esc} -dependent dust attenuation) and the LMC attenuation law. The different colors represent LyC escape fractions $f_{\text{esc}} = 0.3$ (red), 0.7 (green) and 0.9 (blue). Open circles represent scenario B and darker dots the completely dust-free case. While the predicted β distribution in scenario B approaches that of the dust free-case (identical for both scenarios A and B) at high f_{esc} , there are lingering effects on the $\text{EW}(\text{H}\beta)$ distribution because of the contribution to the $\text{H}\beta$ continuum from direct, unattenuated starlight, with lower $\text{EW}(\text{H}\beta)$ as a result.

$z > 6$, the dust continuum gets redshifted into the sub-mm regime and is hence outside the wavelength range of JWST. In the case of the very brightest reionization-epoch galaxies, the dust continuum can be probed by ALMA (e.g. Watson et al. 2015), but the sensitivity limits of ALMA makes this impossible for the vast majority of $z > 6$ galaxies within reach of JWST/NIRSpec. ALMA observations of the redshifted dust continuum is far less challenging at $z \approx 3$ (Scoville et al. 2016), where the opacity of the IGM still allows direct detection of escaping LyC. Hence, it should at least be possible to assess how pronounced LyC extinction is in bright, high- f_{esc} galaxies ≈ 1 Gyr after cosmic reionization has completed.

4.2. Heavily obscured star formation

Due to the relatively limited wavelength range within reach of JWST/NIRSpec for galaxies at $z = 6$ –9 (rest-frame wavelengths 1216 to ≈ 5000 –7100 Å, depending on the exact redshift), it is possible to come up with scenarios that are bound to lead the JWST analysis of such galaxies astray. Objects with very high dust obscuration would represent a particularly troublesome case.

Consider the case where supernovae punch small holes through an extremely dusty and opaque ISM, so that some small fraction f_{esc} of starlight is escaping without any attenuation by gas or dust whatsoever, whereas the rest is subject to very high dust attenuation. This resembles our viewing angle scenario B, but with far more pronounced dust effects outside the holes than considered in our simulations. The unobscured part could then completely dominate the rest-frame ultraviolet/optical light. If the unobscured region is young, the observed spectrum would exhibit a very blue UV slope and extremely weak emission lines – the tell-tale signatures of a very high overall f_{esc} – despite the fact that the global f_{esc} is very low.

In fact, Kimm & Cen (2013) have proposed a model of this type to explain the observed properties of $z = 7$

galaxies, adopting $f_{\text{esc}} = 0.1$ and an optical attenuation of $A_V = 1.8$ magnitudes over the attenuated regions. As in the case of direct LyC absorption by dust (Section 4.1), the most direct way to get an observational handle on this scenario would likely be auxiliary observations of the very brightest JWST/NIRSpec targets with ALMA (Cen & Kimm 2014). One may also be able to address this using ensemble statistics. If a significant fraction of star formation is generally completely blocked by dust, then the stellar mass is growing much faster than what is inferred from the rest-frame ultraviolet. By comparing the simultaneous growth of the rest-frame ultraviolet and optical luminosity functions in time, it may then be possible to assess whether this is a dominant mode.

A similar complication could arise for galaxies that have two (or more) blended components with vastly different dust and LyC escape properties. If a high-mass component with $f_{\text{esc}} = 0$ experiences too high attenuation to contribute substantially to the observed JWST/NIRSpec SED, a low-mass, low-obscuration $f_{\text{esc}} > 0$ component could come to dominate the observed SED. In this case, any f_{esc} estimate based on our methods would refer solely to the latter component. In a scenario of this kind, one would also severely underestimate the overall stellar mass of the system.

We stress, however, that very few objects subject to very high obscuration have so far been identified at $z > 6$ – with LFLS3 at $z \approx 6.3$ with $M_{\text{stars}} \approx 5 \times 10^{10} M_{\odot}$ and $A_{UV} \approx 5$ mag (Cooray et al. 2014) being the only compelling case so far. On the contrary, both observations and simulations suggest that the average obscuration is $A_{UV} \lesssim 0.5$ mag in all but the most luminous galaxies at $z > 6$ (e.g. Wilkins et al. 2013; Bouwens et al. 2016).

4.3. Density-bounded nebulae

Zackrisson et al. (2013) discussed two separate mechanisms for LyC leakage – an ionization-bounded nebula with holes and a density-bounded nebula. In this paper, we have only considered the former one, since Zackrisson et al. (2013) argue that the two should give rise to very similar signatures in the $\text{EW}(\text{H}\beta)$ - β diagram. However, the relative strength of emission lines like [OIII]5007 and [OII]3727 (which can both be readily observed with JWST/NIRSpec up to $z \approx 9$) differ in the case of density-bounded nebulae, which means that JWST/NIRSpec observations should not only be able to constrain f_{esc} , but also provide the handle on the dominating mode of LyC escape mechanism from galaxies in the reionization epoch. Observations of a galaxy with extreme LyC leakage at $z \approx 3.2$ presented by Vanzella et al. (2016) and de Barros et al. (2016) already support that the leakage is happening through a density-bounded nebula, and the properties of the interstellar medium of the $z \approx 7$ galaxy studied in [OII]88 μm and [CII]158 μm by Inoue et al. (2016) also appear favorable for LyC leakage through this mechanism. For this reason, it would be valuable to extend the present work to include density-bounded nebulae. While this extension is straightforward, it also involves more free parameters, since the oxygen lines are also sensitive to the ionization parameter and the relative oxygen abundance. We do, however, intend to revisit such models in a future paper.

4.4. Anisotropic LyC leakage

Simulations suggest that LyC leakage may be highly anisotropic (Paardekooper et al. 2015; Cen & Kimm 2015), so that even though the global f_{esc} may be significant, the parts of a galaxy that is facing the observer may exhibit very low LyC escape. If so, this would complicate the use of methods aiming to constrain f_{esc} using absorption lines, since these are measuring the covering fraction of foreground gas. One could for instance imagine a galaxy in which absorption lines suggest complete coverage and hence zero LyC leakage, whereas extremely high LyC leakage is taking place in the opposite direction. The same problem also plagues direct detections of LyC leakage from individual objects at $z \lesssim 4$, since these are biased by the LyC fraction that happens to be escaping in the direction of the observer.

As discussed in Sections 2.2 and 3.3, our method would be able to detect the signatures of LyC leakage even in the case of highly anisotropic escape, albeit with caveats. In the case of minor dust attenuation, anisotropic LyC leakage would not be a problem, since nebular emission from all sides of the galaxy should be able to reach the observer. Hence, our method should provide a better handle of the *global* escape fraction of galaxies. However, scenarios involving high obscuration coupled to anisotropic leakage (as discussed in Section 4.2) would introduce a directional bias on the f_{esc} inferred by our method as well.

4.5. Stochastic IMF sampling

The simulated SEDs presented in this paper are based on assumption that the IMF is fully sampled, which is a safe approximation for high-mass stellar populations. For low-mass systems, however, the incomplete sampling of the IMF may lead to stochastic variations between the ionizing and non-ionizing continuum fluxes, which would complicate attempts to estimate f_{esc} based on the equivalent width of emission lines from individual objects. IMF sampling effects are negligible for objects with star formation rates $\text{SFR} \gtrsim 1 M_{\odot} \text{ yr}^{-1}$ (Forero-Romero & Dijkstra 2013; da Silva et al. 2014), which for our simulated galaxies at $z = 7$ correspond to $m_{\text{AB}} \leq 28.5\text{--}29.0$ at rest-frame wavelengths around 1500 Å. In the absence of gravitational lensing, JWST/NIRSpec is not likely to be able to push beyond this limit (Jensen et al. 2016). However, a strongly lensed galaxy that appears at this limit could have $\text{SFR} \ll 1 M_{\odot} \text{ yr}^{-1}$, at which point stochastic IMF sampling effects would start to matter. At this point, the method proposed for estimating f_{esc} would become unreliable for individual objects. The typical f_{esc} in a population of galaxies could in principle still be inferred, but this requires that one takes the predicted distribution of observed properties as a function of f_{esc} into account, and corrects for the fact that the galaxies with the most massive stars are more easily detectable.

4.6. LyC absorption in low-density circumgalactic gas

The method for constraining f_{esc} in this paper and in Zackrisson et al. (2013) is based on notion that the LyC absorbed by gas within galaxies should be reflected in the strength of rest-frame UV/optical emission lines relative to the continuum at these wavelengths (which stems both from direct starlight and free-bound/free-free processes

in the interstellar medium). However, in simulations, the radial delimitator at which a LyC photon is considered to have reached the IGM is traditionally placed at the dark halo virial radius, which means that the LyC photon not only needs to escape from the dense interstellar medium within galaxies, but also needs to make it past neutral gas in the circumgalactic medium, which may have much lower density. When the density drops below $n(\text{H}) \approx 0.1 \text{ cm}^{-3}$, the hydrogen recombination time scale becomes $\gtrsim 1 \text{ Myr}$, which means that the recombination flux per unit time will be much lower than in the denser interstellar medium, and that changes in the stellar LyC output will be reflected in the recombination emission lines with a substantial time delay. As an example of the potential problem that this could introduce, consider an extreme scenario in which a sudden surge of star formation boosts the LyC flux of a stellar population and produces a blue rest-frame stellar ultraviolet continuum, yet all LyC photons are absorbed in low-density, circumgalactic gas. This could result in a situation in which $f_{\text{esc}} \approx 0$, yet the long recombination timescale ensures extremely weak emission lines, suggesting $f_{\text{esc}} \approx 1$. Simulations of the covering fraction and density of neutral gas in the circumgalactic medium of galaxies at $z > 6$ would be very useful to assess how serious this problem is likely to be. Of course, since the problem is fundamentally due to a mismatch between what is measured in observations and simulations, the issue can be completely evaded by simply redefining the threshold radius at which LyC escape is assumed to have occurred in simulations to provide a better match between the two.

5. SUMMARY

Our results can be summarized as follows:

- As part of the LYCAN project, we have generated a large grid of synthetic SED of $z = 7\text{--}9$ galaxies drawn spectra from cosmological simulations, in a wavelength range relevant for JWST/NIRSpec observations at these redshifts. These models, which are intended for the planning of JWST observations and for training data analysis tools, include a number of different options concerning LyC leakage, stellar evolution, dust attenuation and observational noise, and are publicly available.
- We demonstrate, that the method proposed by (Zackrisson et al. 2013) constrain the LyC leakage of reionization-epoch galaxies using indirect spectral signatures (emission lines and continuum) in JWST/NIRSpec spectra seems to hold even in the light of variations in star formation history and metallicity at the level seen in the simulations. Even very simple combinations of diagnostics like the slope of the UV continuum and the strength of the $\text{H}\beta$ emission line allow the identification of extreme ($f_{\text{esc}} > 0.5$) LyC-leaking galaxies (section 3.1). Broadly speaking, such objects are expected to exhibit rest-frame $\text{EW}(\text{H}\beta) \leq 30 \text{ Å}$.
- Uncertainties in dust attenuation, the effective attenuation law and in stellar evolution (e.g. the role of binary evolution and stellar rotation) at $z > 6$ convert into systematic uncertainties in the

f_{esc} inferred from individual galaxies, but upcoming observations at both low-to-intermediate redshifts and at $z > 6$ should allow such model uncertainties to be severely constrained (sections 3.1, 3.3 and 4).

- Potential complications that warrant further studies include direct LyC absorption by dust, density-bounded nebulae, and the absorption of LyC gas in low-density circumgalactic gas with very long recombination timescales (section 4).

E.Z acknowledges funding from the Swedish Research Council (project 2011-5349). JPP acknowledges support from the European Research Council under the European Communitys Seventh Framework Programme (FP7/2007-2013) via the ERC Advanced Grant STARLIGHT: Formation of the First Stars (project number 339177)

REFERENCES

- Asplund, M., Grevesse, N., Sauval, A. J., Scott, P. 2009, *ARA&A* 47, 481
- Bergvall, N., Zackrisson, E., Andersson, B.-G., Arnberg, D., Masegosa, J., Östlin, G. 2006, *A&A*, 448, 513
- Bergvall, N., Marquart, T., Way, M. W., Blomqvist, A., Holst, E., Östlin, G., Zackrisson, E. 2016, *A&A* 587, 72
- Borthakur, S., Heckman, T. M., Leitherer, C., Overzier, R. A. 2014, *Science*, 346, 216
- Bouwens, R. J., et al. 2014, *ApJ*, 793, 115
- Bouwens, R. et al. arXiv1606.05280
- Cai, Z.-Y., Lapi, A., Bressan, A., De Zotti, G., Negrello, M., Danese, L. 2014, *ApJ*, 785, 65
- Calzetti D., Kinney A.L., Storchi-Bergmann T. 1994, *ApJ*, 429, 582
- Calzetti, D., et al. 2000, *ApJ*, 533, 682
- Cen, R., Kimm, T. 2014, *ApJ*, 782, 32
- Cen, R., Kimm, T. 2015, *ApJ*, 801, L25
- Charlot, S., Fall, S. M. 2000, *ApJ*, 539, 718
- Cooray, A., et al. 2014, *ApJ*, 790, 40
- da Silva, R. L., Fumagalli, M., Krumholz, M. R. 2014, *MNRAS* 444, 3275
- de Barros, S., et al. 2016, *A&A* 585, 51
- Dopcke, G., Glover, S. C. O., Clark, P. C., Klessen, R. S. 2013 *ApJ*, 766, 103
- Duncan, K., Conselice, C. J. 2015, *MNRAS*, 451, 2030
- Eldridge, J. J., Stanway, E. R. 2009, *MNRAS*, 400, 1019
- Ferland, G. J., et al. 2013, *Revista Mexicana de Astronomia y Astrofisica* 49, 137
- Ferrara, A., Loeb, A. 2013, *MNRAS*, 431, 2826
- Fernandez, E. R., Dole, H., Iliev, I. T. 2013, *ApJ*, 764, 56
- Finlator, K., Oppenheimer, B. D., Davé, R. 2011, *MNRAS*, 410, 1703
- Finlator, K., Muñoz, J. A., Oppenheimer, B.D., Oh, S. P., Özel, F., Davé, R. 2013 *MNRAS* 436, 1818 (F13)
- Forero-Romero, J. E., Dijkstra, M. 2011, *MNRAS*, 428, 2163
- Gnedin, N. Y., Kravtsov, A. V., Chen, H.-W. 2008, *ApJ*, 672, 76
- Gnedin, N. 2014, *ApJ*, 793, 29
- Hartley, B., Ricotti, M. 2016, arXiv1602.06302
- Hirashita, H., Buat, V., Inoue, A. K., 2003, *A&A*, 410, 83
- Inoue, A. K. 2001, *AJ*, 122, 1788
- Inoue, A. K., Hirashita H., Kamaya, H. 2000, *PASJ*, 52, 539
- Inoue, A. K., Hirashita H., Kamaya, H. 2001, *ApJ*, 555, 613
- Inoue, A. K., Shimizu, I., Iwata, I., Tanaka, M. 2014, *MNRAS*, 442, 1805
- Inoue, A. K., et al. 2016, *Science*, 352, 1559
- Izotov, Y. I., Orlitova, I., Schaerer, D., Thuan, T. X., Verhamme, A., Guseva, N., Worseck, G. 2016a, *Nature*, 529, 178
- Izotov, Y. I., Schaerer, D., Thuan, T. X., Worseck, G., Guseva, N. G., Orlitova, I., Verhamme, A. 2016b, arXiv1605.05160
- Jaskot, A., Ravindranath, S. 2016, arXiv1610.03778
- Jaacks, J., Nagamine, K., Choi, J. H. 2012, *MNRAS*, 427, 403
- Jensen, H., Zackrisson, E., Pelckmans, K., Binggeli, C., Ausmees, K., Lundholm, U 2016, *ApJ*, 827, 5
- Jones, T. A., Ellis, R. S., Schenker, M. A., Stark, D. P. 2013, *ApJ*, 779, 52
- Kimm, T., Cen, R. 2014, *ApJ*, 788, 121
- Kimm, T., Cen, R. 2013, *ApJ*, 776, 35
- Kimm, T., Cen, R., Devriendt, J., Dubois, Y., Slyz, A. 2015, 451, 2900
- Kroupa, P. 2001, *MNRAS*, 322, 231
- Leethochawalit, N., Jones, T. A., Ellis, R. S., Stark, D. P., Zitrin, A. 2016, arXiv1606.05309
- Leitet, E., Bergvall, N., Hayes, M., Linné, S., Zackrisson, E. 2013, *A&A*, 553, 106
- Leitherer C., et al. 1999, *ApJS*, 123, 3
- Leitherer, C., Ekström, S., Meynet, G., Schaerer, D., Agienko, K. B., Levesque, E. M. 2014, *ApJS*, 212, 14L
- Leitherer, C., Hernandez, S., Lee, J. C., Oey, M. S. 2016, *ApJ*, 823, 64L
- Levesque, E. M., Leitherer, C., Ekstrom, S., Meynet, G., Schaerer, D. 2012, *ApJ*, 751, 67
- Ma, X., Kasen, D., Hopkins, P. F., Faucher-Giguere, C.-A., Quataert, E., Keres, D., Murray, N. 2015, *MNRAS*, 453, 960
- Ma, X., Hopkins, P. F., Kasen, D., Quataert, E., Faucher-Giguere, C.-A., Keres, D., Murray, N. 2016, *MNRAS*, 459, 3614
- Matthee, J., Sobral, D., Best, P., Khostovan, A. A., Oteo, I., Bouwens, R., Röttgering, H. 2016, arXiv1605.08782
- Mitra, S., Choudhury, T. R., Ferrara, A. 2016, arXiv1606.02719
- Nakajima, K., Ouchi, M. 2014, *MNRAS*, 442, 900
- Oesch, P. A., et al. 2016, *ApJ*, 819, 129
- Paardekooper, J.-P., Khochfar, S., Dalla, C. V. 2013, *MNRAS*, 429, L94
- Paardekooper, J.-P., Khochfar, S., Dalla Vecchia, C. 2015, *MNRAS*, 451, 2544
- Pei, Y. C. 1992, *ApJ*, 395, 130
- Price, L. C., Trac, H., Cen, R. 2016, arXiv1605.03970
- Price, S. H., et al. 2014, *ApJ*, 788, 86
- Puglisi, A., et al. 2016, *A&A*, 586, 83
- Raiter, A., Schaerer, D., Fosbury, R. A. E. 2010 *A&A* 523, 64
- Reddy, N. et al. 2016 arXiv1606.03452
- Safrank-Shrader, C., Milosavljevic, M., Bromm, V. 2014, *MNRAS*, 438, 1669
- Scoville, N. et al. 2016 *ApJ*, 820, 83S
- Shapely, A. E., et al. 2016, arXiv1606.00443
- Shimizu, I., Inoue, A. K., Okamoto, T., Yoshida, N. 2014, *MNRAS* 440, 731 (S14)
- Stanway, E. R., Eldridge, J. J.; Becker, G. D. 2016, *MNRAS*, 456, 485
- Stasinska, G., Izotov, Y., Morisset, C., Guseva, N. 2015, *A&A*, 576, 83
- Sun, G., Furlanetto, S. R. 2016, *MNRAS*, 460, 417
- Topping, M. W., Shull, J. M. 2015, *ApJ*, 800, 97
- Vanzella, E., et al. 2016, arXiv:1602.00688
- Vasei, K., et al. 2016, *ApJ*, submitted (arXiv1603.02309)
- Vázquez, G. A., & Leitherer, C. 2005, *ApJ*, 621, 695
- Watson, D., Christensen, L., Knudsen, K. K., Richard, J., Gallazzi, A., Michalowski, M. J. 2015, *Nature*, 519, 327
- Wilkins, S. M., Bunker, A., Coulton, W., Croft, R., Matteo, T. D., Khandai, N., Feng, Y. 2013, *MNRAS*, 430, 2885
- Wilkins, S. M., Feng, Y., Di-Matteo, T., Croft, R., Stanway, E. R., Bouwens, R. J., Thomas, P. 2016, *MNRAS*, 458, L6
- Wofford, A., et al. 2016, *MNRAS*, 457, 4296
- Xu, H., Wise, J. H., Norman, M. L., Ahn, K., O'Shea, B. W. 2016, arXiv1604.07842
- Yajima, H., Li, Y., Zhu, Q., Abel, T., Gronwall, C., Ciardullo, R. 2014, *MNRAS*, 440, 776
- Zackrisson E., Bergvall, N., Leitert, E. 2008, *ApJ*, 676, L9
- Zackrisson E., Rydberg, C.-E., Schaerer, D., Östlin, G., Tuli, M. 2011, *ApJ*, 740, 13
- Zackrisson E., Inoue, A. K., Jensen, H. 2013, *ApJ*, 777, 39